Research Article

Short title: Pyrimidine nucleotide de novo synthesis

Title: Pyrimidine nucleotide availability is essential for efficient photosynthesis, ROS scavenging, and organelle development

[1]Leo Bellin, [2]Michael Melzer, [2]Alexander Hilo, [1]Diana Laura Garza Amaya, [1]Isabel Keller, [3]Jörg Meurer, [1]Torsten Möhlmann

[1]Pflanzenphysiologie, Fachbereich Biologie, Universität Kaiserslautern, Erwin-Schrödinger-Straße, D-67663 Kaiserslautern, Germany
[2]Leibniz Institut für Pflanzengenetik und Kulturpflanzenforschung (IPK), Corrensstrasse 3, 06466 Seeland, OT Gatersleben, Germany
[3]Plant Sciences, Department Biology I, Ludwig-Maximilians-University Munich, Großhaderner Straße 2-4, 82152, Planegg-Martinsried, Germany.

Author for contact:
Dr. Torsten Möhlmann, Universität Kaiserslautern, Pflanzenphysiologie,
Postfach 3049, D-67653 Kaiserslautern, Germany,
moehlmann@biologie.uni-kl.de

ONE-SENTENCE SUMMARY: Impaired pyrimidine nucleotide synthesis results in a low energy state, affecting photosynthesis and organellar ultrastructure, thus leading to reduced growth, reproduction, and seed yield

AUTHOR CONTRIBUTIONS: T.M. conceived and supervised the study, obtained funding, and provided resources. L.B. generated all mutants and performed characterization, M.M. performed morphological and ultrastructure analysis, A.H. performed metabolite measurements, D.L.G.A. performed growth, carbohydrate and gene expression analysis, I.K. advised and interpreted ROS determination, J.M. advised and interpreted determination of photosynthesis parameters. T.M. and L.B. wrote the original draft. All authors reviewed and edited the manuscript.

ABSTRACT

De novo synthesis of pyrimidines is an essential and highly conserved pathway in all organisms. A peculiarity in plants is the localization of the first committed step, catalyzed by aspartate transcarbamoylase (ATC), in chloroplasts. By contrast, the third step in the pathway is catalyzed by dihydroorotate dehydrogenase (DHODH) localized in mitochondria in eukaryotes, including plants. To unravel pathway- and organelle specific functions, we analyzed knock-down mutants in *ATC* and *DHODH* in detail. *ATC* knock-downs were most severely affected, exhibiting low levels of pyrimidine metabolites, a low energy state, reduced photosynthetic capacity and accumulated reactive oxygen species (ROS). Furthermore, we observed altered leaf morphology and chloroplast ultrastructure in the mutants. Although less affected, *DHODH* knock-down mutants showed impaired seed germination and altered mitochondrial ultrastructure. Our results point to an integration of de novo pyrimidine synthesis and cellular energy states via photosynthesis and mitochondrial respiration. These findings highlight the likelihood of further regulatory roles for ATC and DHODH in pathways located in the corresponding organelles.

INTRODUCTION

Pyrimidine nucleotides are fundamental cellular constituents. They serve as building blocks for DNA and RNA, and participate in metabolic processes ranging from sugar interconversion and polysaccharide metabolism to biosynthesis of glycoproteins and phospholipids (Kafer et al., 2004; Garavito et al., 2015). The largest portion of cellular nucleotides is contained in ribosomal RNAs thus affecting translation and growth (Busche et al., 2020).

Pyrimidine biosynthesis is an ancient and evolutionarily conserved biochemical pathway and has been studied intensively in mammalian systems, other eukaryotes and prokaryotes. Yet, studies of this pathway in plants are scarce, especially with respect to its regulation and interactions with other pathways. The first pyrimidine nucleotide, uridine monophosphate (UMP), is synthesized by the *de novo* pathway via enzymatic steps that appear to be invariant in all organisms (Martinussen et al., 2011). In most multicellular eukaryotes, including mammals, some fungi, and insects, the first three steps of the *de novo* pathway are encoded by a single transcriptional unit generating a polyprotein called CAD (Christopherson and Szabados, 1997; Kim et al., 1992). The CAD complex consists of carbamoyl phosphate synthase (CPS), aspartate transcarbamoylase (ATC), and dihydroorotase (DHO) and localizes to the cytosol.

Plant *de novo* pyrimidine biosynthesis follows a distinct gene and cell compartment organization scheme relative to other organisms (Nara et al., 2000; Santoso and Thornburg, 1998). The first three enzymes are encoded by individual and unlinked genes that map to chromosomes 1, 3 and 4, respectively, in Arabidopsis (*Arabidopsis thaliana*) (Williamson and Slocum, 1994; Williamson et al., 1996; Nara et al., 2000). The encoded proteins also exhibit different subcellular localizations (Witz et al., 2012; Witte and Herde, 2020). Although the first step in the pathway is encoded by CPS, ATC is responsible for the first committed step in plant pyrimidine biosynthesis. It localizes to the chloroplast stroma and catalyzes the production of carbamoyl aspartate (CA), which is then likely exported to the cytosol and converted to dihydroorotate by the cytosolic DHO enzyme. Evidence is mounting for an association between the ATC and DHO enzymes at the chloroplast membrane (Doremus and Jagendorf, 1985; Witte and Herde, 2020; Trentmann et al., 2020), which would allow for metabolite channeling across cellular compartments. The next step in *de novo* pyrimidine biosynthesis involves the enzyme dihydroorotate dehydrogenase (DHODH), which resides in the mitochondrial intermembrane space, where it is coupled to the respiratory chain. DHODH facilitates the closure of the pyrimidine ring to generate orotate (Zrenner et al., 2006; Witz et al., 2012).

DHODH from multicellular eukaryotes, including Arabidopsis, requires ubiquinone as electron acceptor for activity, provided by the mitochondrial respiratory chain. Besides exhibiting a mitochondrial targeting peptide at its N terminus, Arabidopsis DHODH contains a transmembrane helix that anchors the protein into the inner mitochondrial membrane (Ullrich et al. 2002; Löffler et al., 2020).

The last two enzymatic steps leading to the production of the first nucleotide, UMP, are catalyzed by the bifunctional cytosolic protein uridine-5′-monophosphate synthase (UMPS) (Nasr et al., 1994; Zrenner et al., 2006). The reason behind the distinct localization of each enzyme, in particular the chloroplast localization of ATC, is currently unclear. However, the upstream reaction is catalyzed by the plastid-localized enzyme CPS, which provides the precursor carbamoyl phosphate (CP) for pyrimidine and arginine synthesis. In contrast to plants, animals possess two CPS isoforms with distinct localizations: one CPS resides in mitochondria and serves the urea cycle, while the other CPS isoform acts in *de novo* pyrimidine biosynthesis in the cytosol (Lehninger, 1994). UMP is a potent feedback inhibitor for plant CPS and ATC activity (Moffatt and Ashihara, 2002), but how plastidic and cytosolic UMP pools equilibrate to allow such regulation remains unknown. An unknown pyrimidine nucleotide transporter has been hypothesized to reside at the plastid envelope to bring UMP into the organelle, in addition to a supply of pyrimidines from the plastidic pyrimidine salvage pathway (Ohler et al., 2019; Schmid et al., 2019).

RNA interference (RNAi) was previously utilized to knock down the expression of *ATC* in Arabidopsis and *ATC* and *DHODH* in Solanaceous species (Schröder et al., 2005; Chen and Slocum, 2008). A clear growth limitation was observed when *ATC* transcript levels were reduced by at least 50%, or 90% for *DHODH* (Schröder et al., 2005). However, a more detailed analysis of *de novo* pyrimidine biosynthesis is lacking, especially in the context of integrating the contribution of each organelle. To fill this gap, we performed an in-depth analysis of knock down mutants in pyrimidine biosynthesis genes *ATC* and *DHODH*. We revealed the common set of plant responses due to reduced pyrimidine nucleotide availability and unraveled potential specific responses related to metabolism in the corresponding organelles.

Results

The aim of this work was to obtain a detailed understanding of the consequences of downregulation of pyrimidine de novo synthesis. The approach used for this included 1. knocking down ATC, catalyzing the first committed step in the pathway and 2. knocking down DHODH, catalyzing the third step. As both enzymes are located in organelles, chloroplasts and mitochondria, respectively, it was intended to unravel potential interactions with processes taking place in the respective organelle. In addition to knock-down lines for ATC (denominated *atc#1* and *atc#2*) which were already preliminarily described (Bellin et al., 2021) two additional knock-down lines for DHODH (denominated as *dhodh#1* and *dhodh#2*) were created in this work. ATC knock-down mutants showed 17% and 12% residual transcript levels leading to 34% and 12% residual protein in *atc#1* and *atc#2*, respectively. (Bellin et al., 2021; Figure 1A, B). For *dhodh#1* and *dhodh#2* residual transcript accumulation was 18% and 6% (Figure 1C). Here, we present a thorough analysis of these plant lines, which showed different degrees of growth restrictions. Initially, the morphological differences between those lines are described at the macroscopic level, followed by analysis at subcellular level by microscopic inspection of chloroplasts and mitochondria and further an in-depth analysis of photosynthesis parameters, ROS stress and metabolite contents.

A reduced capacity for de novo synthesis impairs plant growth and development

It was an obvious observation that *ATC* mutants were more severely impaired in growth and development compared to *DHODH* mutants. In comparison to the Col-0 control plants all mutant lines showed a delay in the emergence of the first true leaves (Figure 1D).

Early delays in development were followed by retarded and reduced growth in the vegetative and reproductive growth phase (Figure 1D,E; Supplemental Figure 1) resulting in lower fresh weights (Figure 1F) and smaller rosette diameters (Supplemental Figure 1A). After six weeks of growth, *atc#1* and *atc#2* only reached 18% and 6% of the fresh weight of control plants, while *DHODH* lines reached 72% and 45% (Figure 1F). In addition, the *ATC* mutant lines exhibited a significant reduction in the maximal primary stem length. Col-0 plants reached a maximum height of 40.5 cm, *atc#1* and *atc#2* only reached a height of 15.7 and 4.4 cm and *dhodh#1* and *dhodh#2* of 24.8 cm and 8.1 cm respectively (Supplemental Figure 1B,C).

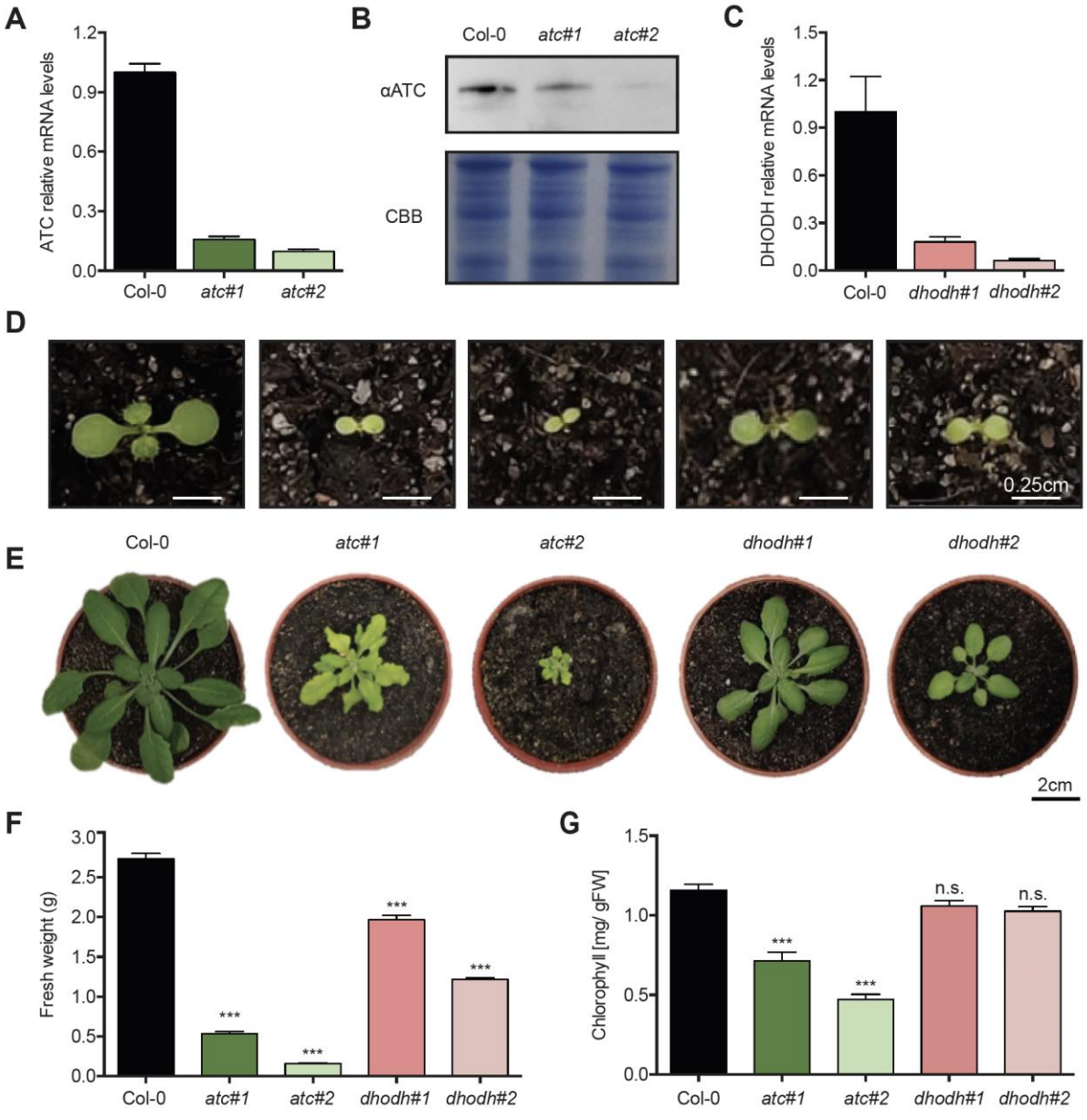

Figure 1. Silencing the ATC and DHODH inhibits vegetative and reproductive growth. A, Relative transcript levels of ATC in Col-0 and corresponding knock-down lines (n = 9). Col-0 control was set to 1 after all transcripts were normalized to actin. B, Immunoblot of ATC protein contents in Col-0 and *ATC* knock-down lines (top) with the corresponding Coomassie-brilliant blue (CBB) staining as a loading control (bottom). C, Relative transcript levels of *DHODH* in Col-0 and corresponding knock-down lines (n = 9). D, E, Typical examples of Col-0 and ATC or DHODH knock-down lines grown for one (D) and four weeks (E) in a 14h light/10h dark regime. F**,** Fresh weight (n = 10) from six week old plants and G, chlorophyll quantification (n = 6) from four weeks old overground plant material. Data points represent means of biological replicates (n) ± SE. Asterisks depict significant changes between the different lines referring to Col-0 according to one-way ANOVA test followed by the Dunnett's multiple comparison test (*** = p<0.001). A, B, F (*atc-1* and *2*) reproduced from Bellin et al., 2021

Additionally, a leaf chlorosis was observed for the *ATC* mutant lines, but not for DHODH lines (Figure 1D,E). Corresponding total chlorophyll contents were significantly reduced by 41% and 61% in leaves of *atc#1* and *atc#2*, respectively (Figure 1G). In contrast, leaves of DHODH mutant plants did not show a significant alteration in chlorophyll contents.

Tissue specific expression of ATC and DHODH are similar

To examine the tissue-specific expression of *Arabidopsis ATC* and *DHODH* in detail, transgenic plants were produced carrying transcriptional fusions of the GUS open reading frame with *PYRB* or *PYRD* promoters. For the ATC-GUS and DHODH-GUS fusions, 965 or 1140 bp upstream of the respective ATG start codons were chosen. For each construct 5 independent primary transformed (F2) lines were inspected. Typical examples of GUS staining patterns are shown in Figure 2.

In all experiments, *PYRB::GUS* and *PYRD::GUS* reporter constructs exhibited similar expression patterns. A developmental time course revealed that ATC (Figure 2A-H) and DHODH (Figure 2I-P) are highly expressed during seed germination and early seedling development (Figure 2A-C and I-K). Thereby, young seedlings from both lines showed a similar staining pattern in differentiating, rapidly dividing and expanding cells like roots, developing shoot apex and the first emerging organs, the cotyledons.

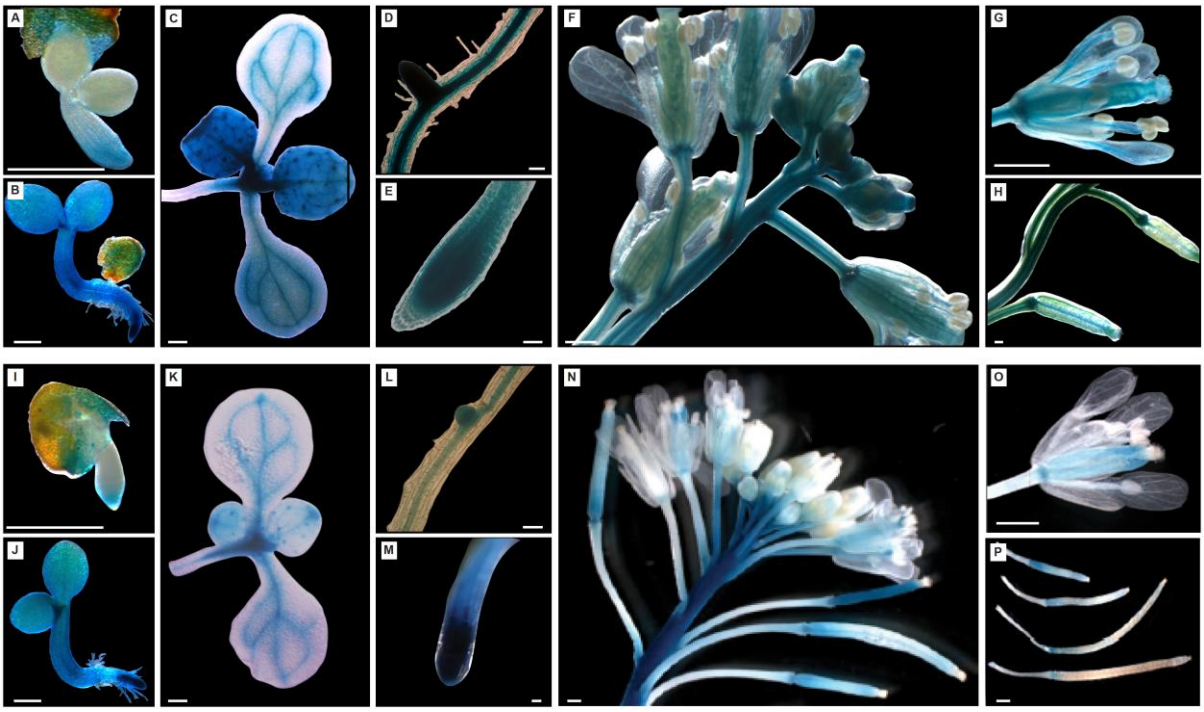

Figure 2. Histochemical analysis of expression patterns of *PYRB* (ATCase; A-H) and *PYRD* (DHODH; I-P) in developing transgenic Arabidopsis plants. Images are shown for two (A, I) and four (B, J) days old seedlings. Shoots of two weeks old plants (C, K) corresponding lateral roots (D, L) and root tips (E, M). The inflorescence of adult plants (F, N) and in closer view flower (G, O) and siliques (H, P) are shown. Scale bars = 0.5 mm (A-C, F-K, N-P) or = 50 µm (D, E, L, M).

During the first week of seedling development the staining increases. Whereas two-days old seedlings showed massive staining in the root elongation- and the root hair zone, in 4-days old seedlings all tissues were already stained intensively (Figure 2A,B,I,J). In two-week,

old seedlings GUS signal could be detected over the whole cotyledons (Figure 2C,K). Furthermore, the vasculature showed intense staining in cotyledons. The whole leaf area including vasculature and punctate structures, was stained in the first true leaves (Figure 2C, K). Staining of the leaf vasculature remained high during leaf development, in contrast, staining in the mesophyll weakened with increasing age of the leaves (Supplemental Figure S2). Moreover, intensive staining was also visible in primary and secondary roots as well as in root tips (Figure 2 D,E,l,M).

However, as the transgenic plants mature, strong staining was observed very early in developing floral primordia and buds (Figure 2F,N). By that, in flowers, GUS staining was visible in sepals, anther filaments and throughout pistil tissues in ATC- and DHODH-GUS plants (Figure 2F,G,N,O). During silique development and seed embryogenesis, various degrees of staining were observed. While in the silique itself and the walls surrounding the developing embryo the GUS staining could be detected, the developing seeds were not stained (Figure 2H,P). To conclude, GUS reporter system analysis revealed that both, ATC and DHODH, are expressed throughout plant development in nearly all of the analyzed tissues.

Embryo-, seed development and seed germination are altered in knock-down lines in pyrimidine *de novo* synthesis

Since clear differences in size and number of siliques between the lines were already visible by eye, seed development and yield were analyzed more closely. Silique length was reduced in all mutant lines. Compared to control plants the silique length in *ATC* knock-down lines was reduced to 60.5% and 42.6%, and for *DHODH* knock-down lines down to 80.7% and 60.7% (Supplemental Figure 3A,B). When developing siliques of mutant lines were opened, empty positions with aborted seeds (red asterisks) and less colored seeds (lacking embryos; white arrows) were visible in all knock-down lines, but not in Col-0 controls (Figure 3A). The number of seeds per silique was found to be reduced in all knock-down lines, but strongest in *atc#2* with only 22.1% of residual viable seeds (Figure 3B). In *atc#1*, *dhodh#1* and *dhodh#2* the number of viable seeds per silique was reduced as well, to 75.9%, 78.8% and 53%, respectively. Whereas Col-0 plants contained 0.8 ± 0.15 aborted seeds per silique, siliques of *atc#1* and *atc#*2 contained 3.16 ± 0.18 and 6.04 ± 0.54 aborted seeds, respectively (Figure 3B).

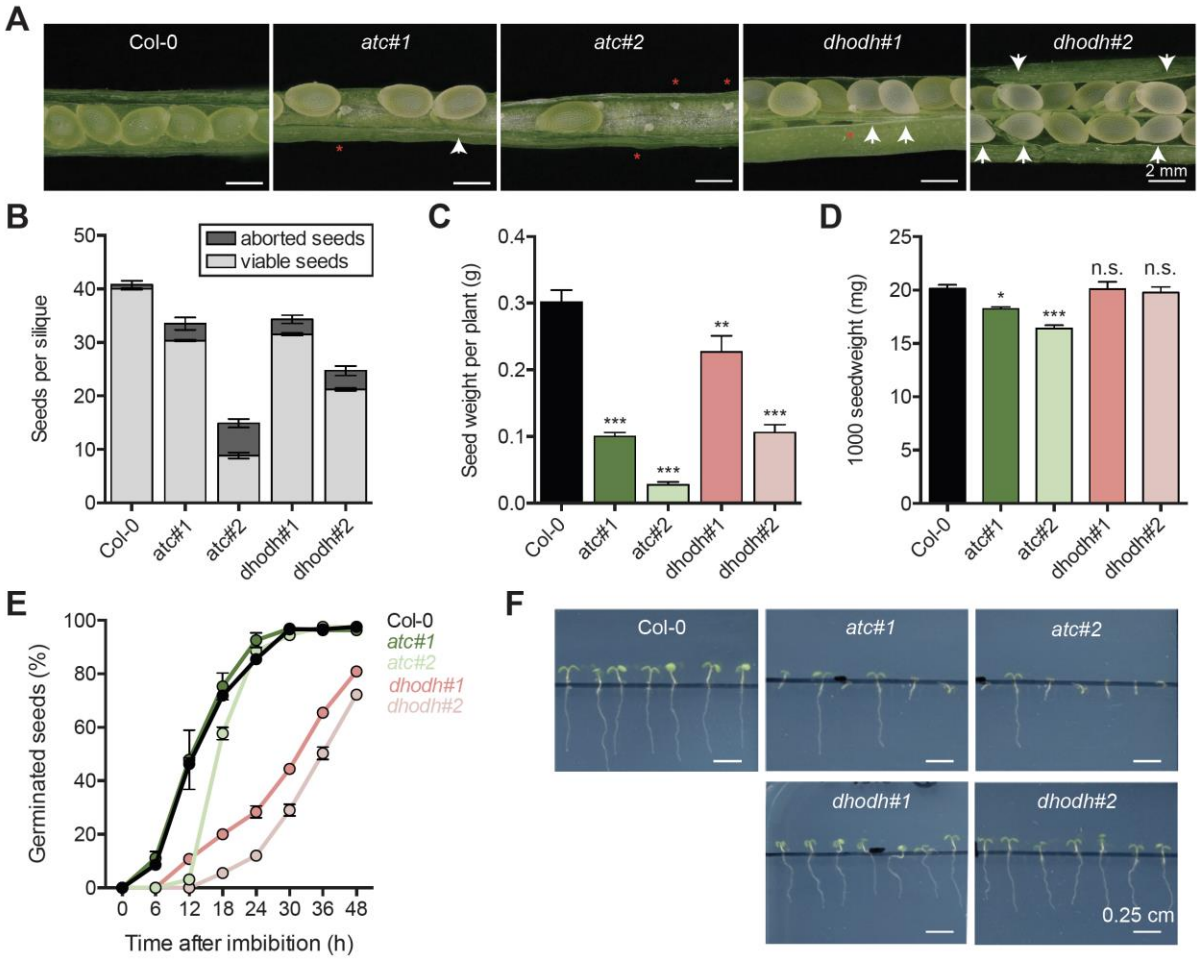

Figure 3. Embryo and seed development. A, Representative siliques of Col-0, *ATC* and *DHODH* knock-down lines showing viable, aborted seeds (red Asterix) and lacking embryos (white arrow). B, Number of viable and aborted seeds per silique. Seeds of 50 siliques from 5 plants per line were counted. C, Seed weight per plant (n=11). D, For determination of 1.000 seed weight 10 different plants per line were used. (E and F) Seed germination assays were performed on ½-MS media in a 14h light/10h dark regime (n=9). (E) Germination rate monitored in a time course of 48 hours after imbibition. F, Root growth was quantified with six-day old seedlings. Data points represent means of biological replicates ± SE. Asterisks depict significant changes between the different lines referring to the WT according to one-way ANOVA followed by the Dunnett's multiple comparison test (* = $p < 0.05$, ** = $p < 0.01$, *** = $p < 0.001$).

This phenotype was less severe for *dhodh#1* and *dhodh#2* with 2.8 ± 0.23 and 3.52 ± 0.26 missing seeds and seeds without embryos per silique (Figure 3B). Shorter siliques as well as increased numbers of aborted seeds per silique in knock-down lines resulted in reduced yield of mature seeds per plant. The weight of seeds per plant was reduced by 66% and 91% for *atc#1* and *atc#2* and by 24% and 65% for *dhodh#1* and *dhodh#2* in comparison to the Col-0 (Figure 3C). Analysis of the 1.000-seed weight of mature, dried seeds revealed a reduced seed weight in both *ATC* knock-down lines, whereas in *DHODH* knock-down plants the 1.000-seed weight was comparable to the wild type (Figure 3D).

To determine whether the seed development impacts mature seed properties, the seed germination was analyzed. Whereas only small alterations were observed between *Col-0* and *ATC* knock-down lines, surprisingly both *DHODH* knock-down lines showed a significant delay in germination (Figure 3E). 30 hours after transfer of seeds to ambient growth conditions, 97% of Col-0 and 93% and 94% of *atc#1* and *atc#2* seeds germinated. For *DHODH* knock-down lines only 44% (*dhodh#1*) and 30% (*dhodh#2*) of the seeds were germinated after the same time (Figure 3E).

Monitoring of root growth revealed that *DHODH* knock-down plants had compensated their germination delay within five days and appeared similar to wild-type plants, whereas the development of *atc#1* and *atc#2* was nearly arrested 5 days after germination (Figure 3F; Supplemental Figure 3C).

Knock-down lines in pyrimidine *de novo* synthesis reveal altered ultrastructure of chloroplasts and mitochondria

Since all mutant lines showed a severely reduced growth, the leaf morphology and cellular ultrastructure were analyzed in detail by means of histology and transmission electron microscopy. For this, we focused on the most affected lines *atc#2* and *dhodh#2*.

Light microscopy analysis of cross sections from mature leaves revealed that leaf thickness in these lines was reduced by approximately 26% and 5% in *atc#2* and *dhodh#2* in comparison to Col-0 (Figure 4A,C,E; Supplemental Figure S4A).

However, whereas the leaf architecture was wild-type like in *dhodh#2*, *atc#2* knock-down lines showed an altered architecture: the layer of palisade parenchyma was disturbed and the intercellular space in the spongy parenchyma was less pronounced. Furthermore, the number of chloroplasts was reduced in *atc#2* (Figure 4A-F).

Chloroplasts and Mitochondria in leaves and the stems of Col-0, *atc#2* and *dhodh#2* differed in their ultrastructural appearance (Figure 4G-O). Transmission electron microscopy (TEM) revealed that chloroplasts of Col-0 (Figure 4G,J) and *dhodh#2* (Figure 4I,L) plants showed well-developed thylakoids, with typical stacked and interconnected grana.

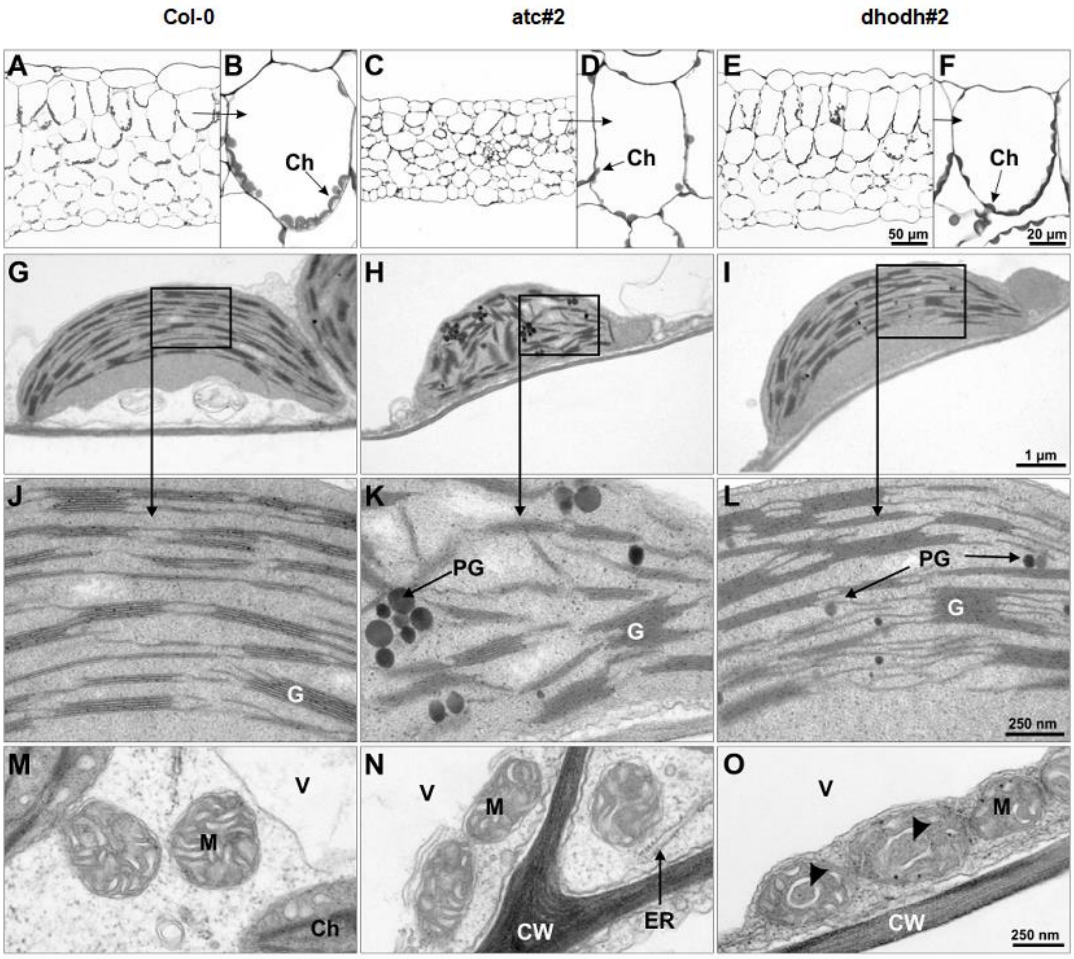

Figure 4. Histological and ultrastructural analysis of rosette leaves of Arabidopsis Col-0, *atc#2*, and *dhodh#2*. Light (**A**-**F**) and transmission electron microscopy images (**G**-**O**) of leaf cross sections of Arabidopsis Col-0 (**A**, **B**, **G**, **J**, **M**), *atc#2* (**C**, **D**, **H**, **K**, **N**) and *dhodh#2* (**E**, **F**, **I**, **L**, **O**). Histological cross section of rosette leaves (**A**, **C**, **E**) with close up of a palisade parenchyma cell (**B**, **D**, **F**). Ultrastructure of chloroplasts with close ups of thylakoids (**G**-**L**) and mitochondria (**M**-**O**) with changes of ultrastructure partly to be observed in dhodh#2 plants (O, arrow heads). Ch, chloroplast; CW, cell wall; ER, endoplasmic reticulum; G, grana; M, mitochondria; PG, plastoglobuli; V, vacuole.

Chloroplasts of *atc#2* mutant plants exhibited changed ultra-structure characterized by loose appearing thylakoids, less dense stacked grana (Figure 4H,K). In addition, their arrangement within the chloroplast was significantly more irregular than in the wild type plants. Further analysis revealed that chloroplasts of *dhodh#2* plants show the same size as the Col-0, whereas the chloroplast size of *atc#2* of is reduced by about 35% (Supplemental Figure 4B). Since the chloroplast ultrastructure was largely unchanged in *dhodh#2;* we intended to determine if the observed phenotype of *DHODH* knock-down lines might be based on defects in the mitochondrial ultrastructure. Thereby, no striking differences in mitochondrial sizes were observed between wild-type and mutant lines (Supplemental Figure 4C).

241 However, compared to Col-0 and *atc#2* plants (Figure 4M,N) about 16% of the
242 mitochondria from *dhodh#2* showed an altered ultrastructure in which the granules were less
243 abundant, and the cristae formed by the inner membrane were reduced. Additionally, the
244 formation of ring like structures has been observed (Figure 4O; black arrows).

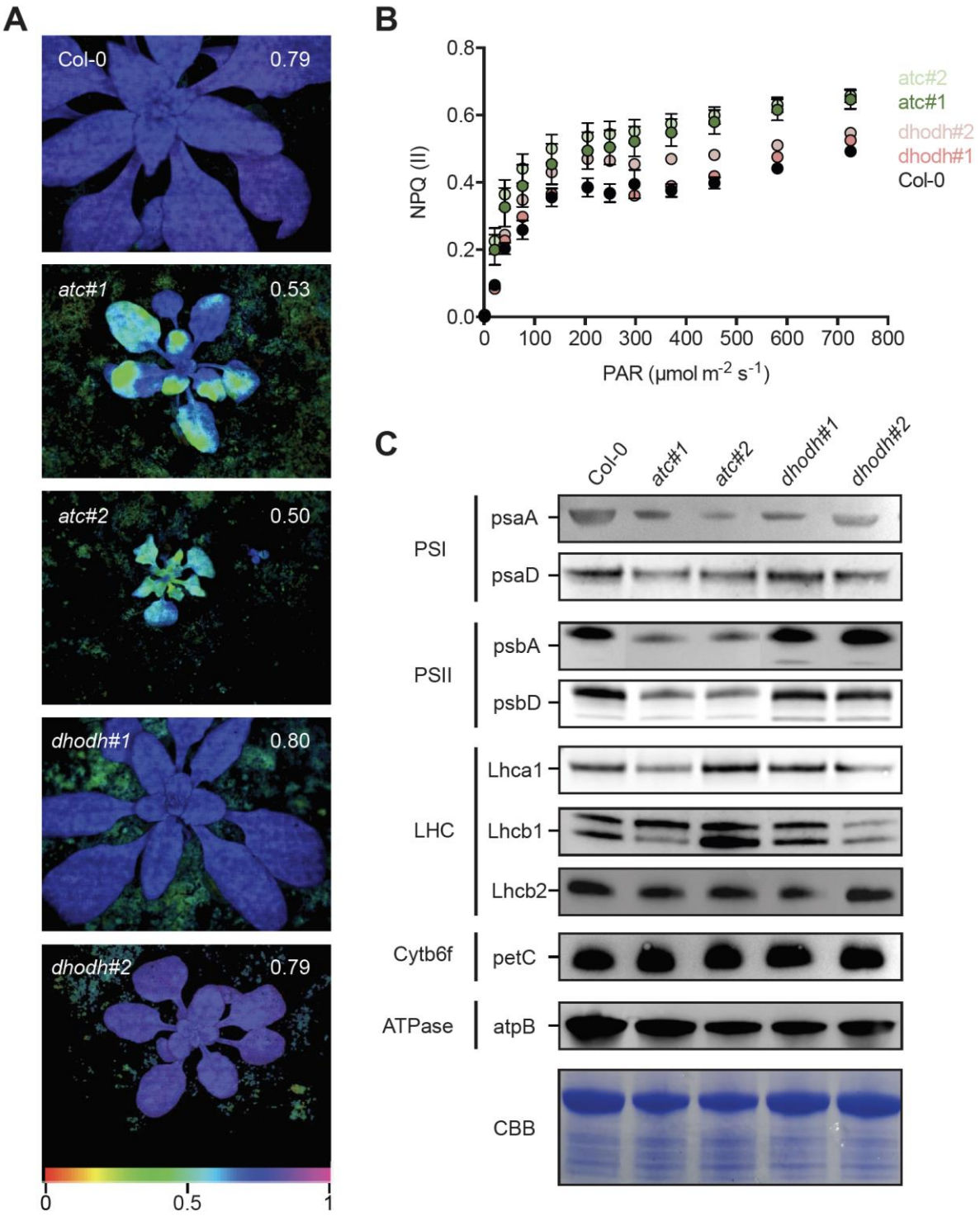

245

246 **Figure 5. ATC activity is required for efficient photosynthesis.** A, False color presentation of
247 effective photosynthesis yield monitored by imaging PAM of four weeks old Col-0 and ATC- and
248 DHODH knock-down mutant plants grown in a 14h light/ 10h dark regime. B, Non-photochemical

quenching (NPQ) measured in a light-response curve (n = at least 8). Data points are means ± SE. C, Immunoblot analysis of photosynthesis related proteins. Proteins were extracted from leaves on a denaturing gel and probed with antibodies as indicated. CBB: Coomassie brilliant blue as a loading control.

Altered photosynthetic efficiency, assimilation, and respiration in knock-down lines in pyrimidine *de novo* synthesis

To determine alterations in the physiology of the lines analyzed, which are fundamental for the observed growth and morphological alterations, we first measured PSII efficiency using chlorophyll fluorescence imaging.

Thereby, Col-0 and *dhodh#1* and *dhodh#2* plants exhibited almost identical maximal photosynthetic efficiency (0.8) whereas *atc#1* and *atc#2* plants showed a reduction to only 0.53 and 0.50, respectively (Figure 5A).

To prevent photosystem II (PSII) from photodamage plants dissipate light energy as heat in the process of non-photochemical quenching (NPQ), thus lowering photosynthetic efficiency (Φ_{PSII}) (Muller et al., 2001; Lambrev et al., 2012). This was reflected by reduced maximal Φ_{PSII} values and higher NPQ in *ATC* knock-down lines (Figure 5B). NPQ values for *dhodh#1* were close to those of control plants, while values of *dhodh#2* were intermediate between Col-0 and *ATC* knock-down lines (Figure 5B).

As we speculate about an effect of reduced pyrimidine nucleotides on rRNA abundance and as related consequence impaired synthesis of photosynthesis related proteins, these were quantified by immunoblotting. The main proteins of photosynthetic reaction centers, PsaA, PsbA, and PsbD were found reduced in *atc#1* and *atc#2* compared to Col-0 and *DHODH* knock-down lines (Figure 5C). PetC was not affected and AtpB was decreased in all mutant lines (Figure 5C).

Reduced photosynthetic efficiency came along with a reduced carbon assimilation rate (*A*) in *atc#1* (74%) and *dhodh#1* and (75%) of the wild type, respectively (Table 1). Respiration (*R)* decreased to 68% and 79% of wild-type level in *atc#1* and *dhodh#1* plant (Table 1).

ROS accumulation challenges the detoxification system in *ATC* knock-down mutants

Altered photosynthetic efficiency can be caused by increased reactive oxygen species (ROS) production (Kato et al, 2009, Su et al., 2018). Thus, the expression of two chloroplast ROS signaling marker genes *zat10* and *bap1* were quantified and found to be massively increased in both *ATC* lines and only slightly in *DHODH* lines (Figure 6A,B).

Table 1. CO_2-Assimilation- and Respiration rate. Mean values ± SE (n=8) are shown. Values (Assimilation and Respiration) for both mutant lines were significantly different to Col-0 (one way Anova with Dunnet posttest).

	Col-0	*atc#1*	*dhodh#1*
Assimilation rate $_{light}$ A (µmol · g^{-1} · s^{-1})	0.0660 ± 0.00754	0.0491 ± 0.00333	0.0493 ± 0.0065
Respiration $_{dark}$ R (µmol · g^{-1} · s^{-1})	0.0364 ±- 0.01020	0.0251 ± 0.00434	0.0292 ± 0.00793

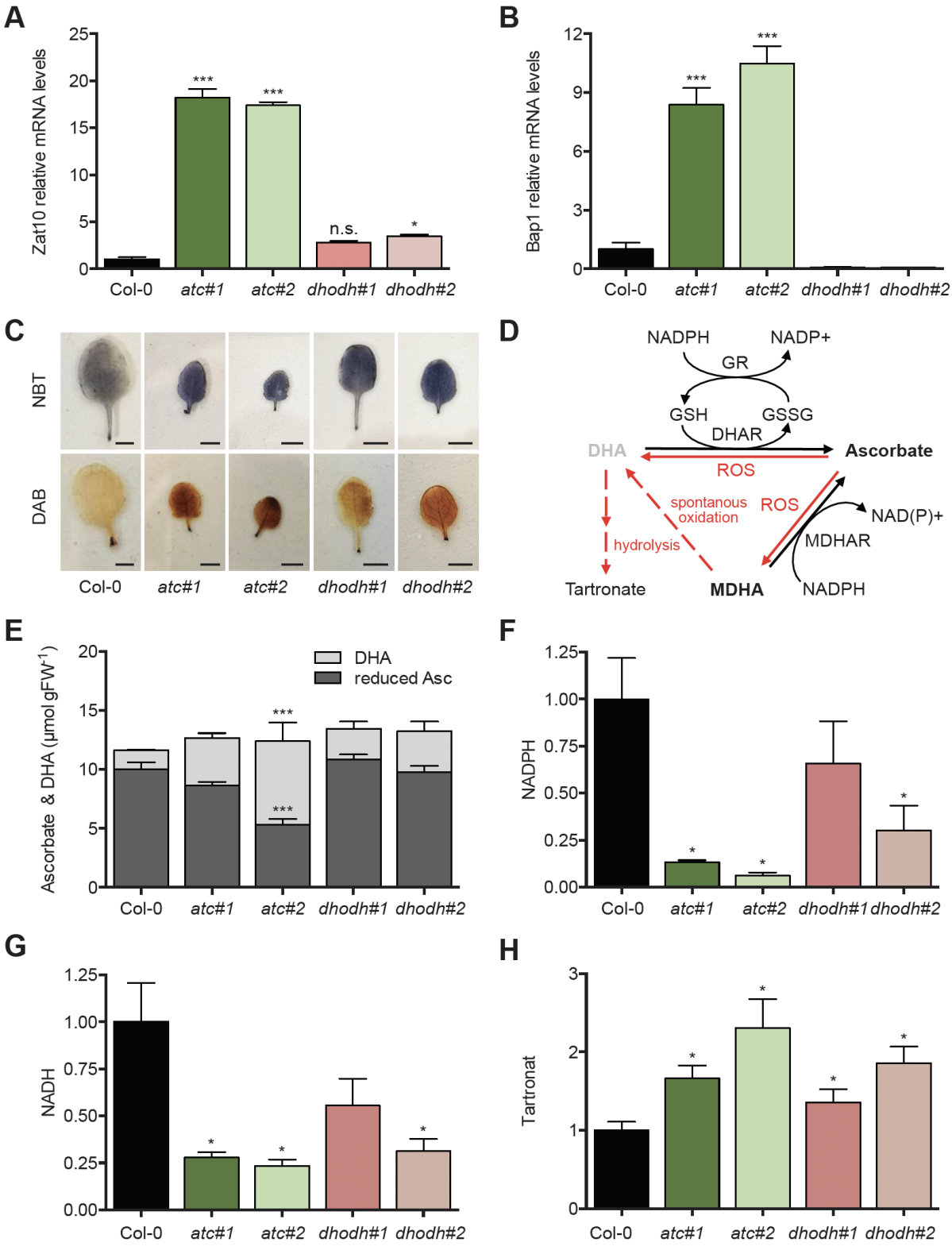

Figure 6. ROS and detoxification-systems A, B, Relative transcript levels of chloroplast ROS signaling markers (A) *zat10* (B) and *bap1* were normalized to actin and Col-0 was set to 1 (n = 3). C, Accumulation of O_2^- and H_2O_2 in 2-week-old plants grown under 14h light/ 10h dark regime visualized by NBT (top panel) and DAB staining (bottom panel) in leaves harvested after 6 hours of light. Images show typical results from the analysis of at least 5 leaves from 3 individually grown plants (Scale bar 0.25 cm). D, Ascorbate is reacting with ROS and can be oxidized to two different forms, dehydroascorbate (DHA) and monodehydroascorbate (MDHA). Ascorbate recycling is catalyzed by a

set of three enzymes: glutathione (GSH)-dependent dehydroascorbate reductase (DHAR), FAD-dependent monodehydro-ascorbate reductase (MDHAR) and glutathione reductase (GR), which regenerates GSH out of oxidized GSSG. (**E**) ascorbate and DHA and (**F**) NADPH (G), NADH and (H) Tartronate contents were determined by LC-MS-measurements (n = 5). Data points of A, B, E and F are means ± SE. Asterisks depict significant changes between the different lines referring to the WT according to one-way ANOVA followed by the Dunnett's multiple comparison test (A, B, E, F) or Wilcoxon Mann-Whitney U-test (G-I) (* = $p < 0.05$, ** = $p < 0.01$, *** = $p < 0.001$)**.**

Superoxide and H_2O_2 were visualized using nitroblue tetrazolium (NBT) and 3,3-diaminobenzidine (DAB; Figure 6C). NBT staining showed that superoxide accumulation was increased in leaves of all knock-down lines relative to Col-0 control plants (Figure 6C, top panel). DAB staining indicates that accumulation of H_2O_2 was strongly increased in *atc#1* and *atc#2*, whereas in the DHODH knock-down lines DAB staining was less intense (Figure 6C, lower panel).

Plants developed different ROS-scavenging strategies involving ascorbate and glutathione as antioxidants to protect cells from oxidative damage (Noctor and Foyer, 1998; Figure 6D). Thereby, at first ascorbate is oxidized by ROS to monodehydro-ascorbate (MDHA) and dehydro-ascorbate (DHA). The regeneration of ascorbate is important to keep a high antioxidative capacity. This is achieved by the two enzymes dehydroascorbate reductase (DHAR) and monodehydroascorbate reductase (MDHAR), using either reduced glutathione or NADPH as reductant (Figure 6D). Concentrations of total ascorbate were higher in all mutant lines, compared to the wild type (Figure 6E). While the ratio of reduced to oxidized ascorbate was comparable in wild-type and *DHODH* lines, it was lowest in *atc#1* and *atc#2* plants (Figure 6E). Both reducing equivalents, NADH and NADPH were massively reduced in both *ATC* lines and *dhodh#2* (Figure 6 F,G) In addition, Tartronate, an intermediate in ascorbate degradation was more abundant in all mutant lines (Figure 6H).

Nucleotides and metabolites from general primary metabolism are altered in *ATC* knock-down mutants

To address the cause of growth restrictions in both types of knock-down lines, we performed an untargeted metabolic profiling of central metabolites using high resolution mass spectrometry. Six-week-old plants grown under long day conditions on soil were chosen for this purpose.

The two intermediates produced by ATC (carbamoyl-aspartate) and dihydroorotase (dihydroorotate), were found to be barely detectable in both knock-down *ATC* lines whereas *DHODH* knock-down lines showed wild-type-like levels. This pattern was congruent with the levels of the downstream generated metabolites UMP and UDP of the pyrimidine *de novo*

pathway. (Figure 7). In both *ATC* knock-down lines the levels of UMP and UDP were significantly reduced to around 50% compared to Col-0 controls.

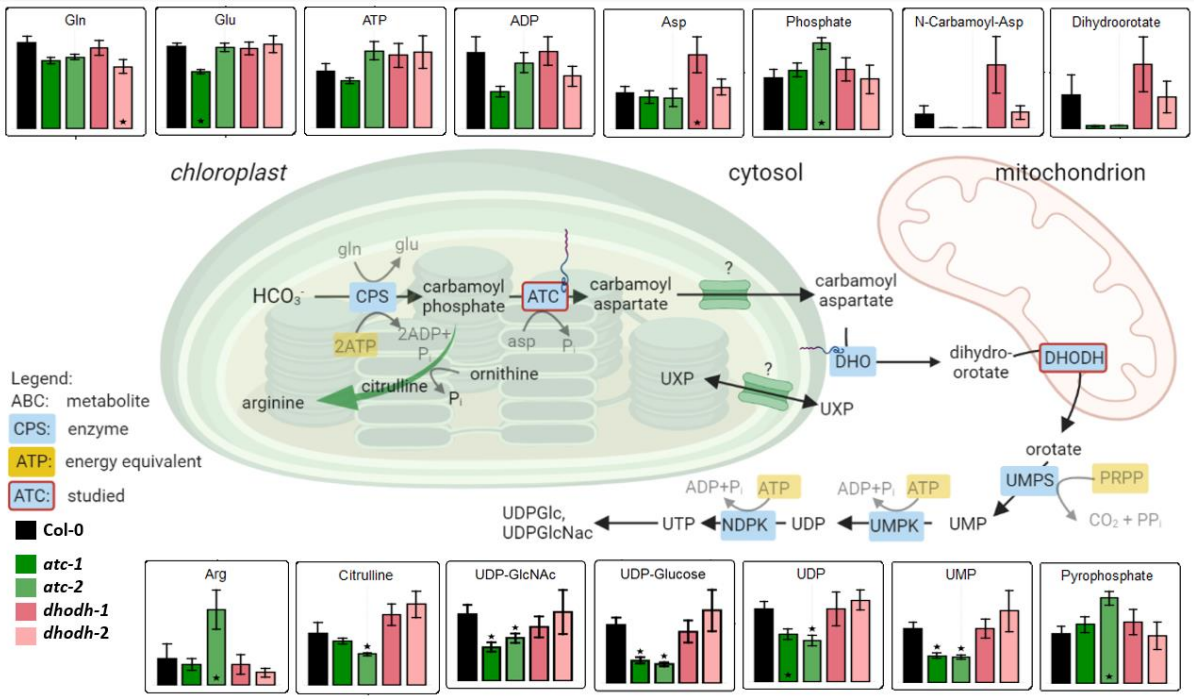

Figure 7. Scheme of pyrimidine de novo synthesis and corresponding metabolites levels. Relative metabolite levels from fully developed leaves are shown, Col-0 (black bars) was set to 1. Green bars indicate *atc#1* (dark green) and *atc#2* (light green) metabolite levels. Red bars indicate *dhodh#1* (red) and *dhodh#2* (light red) metabolite levels as log2-fold changes relative to Col-0. Asterisks indicate significantly (p-value < 0.05, Wilcoxon Mann-Whitney U-test) altered levels. (n=5).

This observation is also supported by a decrease of UTP-activated metabolites in those lines, such as UDP-glucose, a key intermediate in sucrose and cellulose synthesis and in UDP-N-acetyl-D-glucosamine, a glycosyl donor used for protein modification (Figure 7).

This indicates that a reduction of ATC expression down to 17% and below strongly impairs pyrimidine *de novo* synthesis, whereas a decrease of DHODH transcripts to 6% is still tolerated. A drastic drop of pyrimidine metabolites can be causative for the observed growth effects.

Furthermore, it is well known that pyrimidine and purine metabolites must be balanced to support nucleotide and nucleic acid synthesis (Reichard, 1988). Among purine nucleotides, the abundances of AMP and GMP were markedly increased in *atc#1*, *atc#2*, and *dhodh#2*, thus exhibiting a negative correlation to the pyrimidine nucleotides described above. In contrast, ADP and ATP levels were only marginally affected in all lines (Figure 7). Especially *atc#1* exhibits increased levels of the purine breakdown products 2-ureido glycine, allantoate, and allantoin, the latter are suggested to function in attenuating ROS stress (Brychkova et al., 2008).

A number of glucosinolates (glucoraphanin, glucoiberin, glucohirsutin, glucoiberin and glucohesperin), involved in pathogen resistance, were also strongly reduced in *atc#1*, *atc#2*, and *dhodh#2* (Supplemental Figure S5). Moreover, the levels of several intermediates of sugar metabolism, TCA cycle, and glycolysis, were significantly affected in the knock-down lines (Supplemental Figure S6).

Discussion

In this work, we analyzed the function of two enzymes of the *de novo* pyrimidine biosynthesis pathway located in the chloroplast (ATC) and mitochondria (DHODH) by employing corresponding knock-down lines. *ATC* transcript levels were reduced by 84 and 90% relative to wild type in the two analyzed, representative knock-down lines, which corresponded to the lower levels of ATC protein (Figure 1A, B, Bellin et al., 2021) consistent with previous reports (Chen and Slocum, 2008). These lines showed severe growth limitations throughout development. Notably, *DHODH* lines had much weaker phenotypes than *ATC* lines, although both sets of lines were characterized by a comparable reduction in transcript levels (Figure 1A), pointing to a higher control of ATC, catalyzing the first committed step in *de novo* pyrimidine synthesis, relative to DHODH. This observation is in line with previous reports on mutants in *de novo* pyrimidine synthesis from Arabidopsis or solanaceous species, suggested high control of ATC over the pathway (Schröder et al., 2005; Geigenberger et al., 2005; Chen et al., 2008). Because nucleotides are central metabolites in many pathways, a reduced capacity for their synthesis is likely to globally affect the central metabolism.

The levels of carbamoyl aspartate (CA), the product of the ATC reaction and of dihydroorotate, the substrate of the DHODH reaction, , were similar in Col-0 and *DHODH* mutants but were close to the detection limit in both *ATC* lines (Figure 7). We observed a similar pattern with a marked and significant reduction in *atc#1* and *atc#2* lines for further pyrimidine nucleotides such as UMP, UDP, UDP-Glc, and UDP-N-acetyl-D-glucosamine, whereas *DHODH* lines behaved more wild type-like. Reduced levels of pyrimidine metabolites in *ATC* lines were accompanied by increased levels of AMP and GMP, which both show a negative correlation with UMP levels. In addition, free phosphate and pyrophosphate accumulated while the reducing agents NADPH and NADH were massively depleted. Together, these results point to reduced energy availability that likely contributes to the observed growth defects in *ATC* lines.

Photosynthetic yield was clearly reduced in both *ATC* lines, but not in *DHODH* lines (Figure 5A). This reduced photosynthetic efficiency may result from photoinhibition, reflecting a light-induced damage of the PSII reaction center, followed by free radical-induced damage of other photosynthetic components (Järvi et al. 2015). Indeed, we also detected an increased expression of ROS marker genes (Figure 6A,B) and higher ROS levels, as determined by NBT and DAB staining (Figure 6C). Furthermore, the ROS scavenging system was affected, as dihydro-ascorbate levels were higher both *ATC* lines.

NADPH recycling is low under conditions of reduced photosynthetic yield, but the levels of NADH and NADPH are depleted further by the reduction of oxidized ascorbate via the Foyer-Asada-Halliwell pathway (Foyer and Noctor, 2011). These combined effects may thus explain the strongly decreased levels of the NADPH and NADH pools.

How a smaller pool of pyrimidine nucleotides in *ATC* amiR lines and a low energy level led to photoinhibition remains an open question. We hypothesize that a low content of pyrimidine nucleotides and the resulting imbalance in purine nucleotides will negatively affect RNA synthesis, especially that of ribosomal RNAs, since they represent the main sink for nucleotides (Busche et al., 2020). Indeed, nucleotide availability can limit ribosome biogenesis (Brunkhardt et al., 2020) and a resulting low translation efficiency in the chloroplast will have major consequences on the function of the organelle, especially for proteins with a high turnover rate. The most prominent candidate here is D1 from PSII. Insufficient D1 recycling will lead to photoinhibition (Järvi et al., 2015) and ROS accumulation, as observed in *ATC* lines (Figure 5, 6).

Inefficient biosynthesis or repair of photosynthetic proteins (such as integral membrane proteins of the electron transport chain) may drive the observed alteration in chloroplast ultrastructure seen in *ATC* lines, with less dense grana stacks and loose thylakoid structures (Figure 4, Järvi et al., 2015). In addition, a high number of plastoglobuli were observed in *ATC* lines. These electron-dense bodies within chloroplasts are involved in thylakoid lipid remodeling (Rottet et al., 2015), and chlorophyll breakdown (von Wijk and Kessler, 2017). Reduced photosynthetic yield and the activation of ROS detoxification systems may then lead to a low energy state. Furthermore, a low NADPH pool might not be able to redox-activate the thylakoid ATP-synthase (whose protein levels decreased in both *ATC* lines in addition)(Figure 5), thus further exacerbating the low energy state (Carrillo et al., 2016) and impairing plant growth. Why *DHODH* lines did not display the alterations in chloroplasts as described above is not clear, but suggests that the main control nexus of the pathway takes place at the level of ATC. However, we cannot rule out the possibility that the plastid-localized enzyme ATC exerts additional regulatory functions on chloroplast pathways like photosynthesis. In addition, the higher tolerance of plants faced with the down-regulation of *DHODH* relative to *ATC* requires further attention. The expression pattern of the *ATC* and *DHODH* genes did not reveal substantial differences when interrogated with promoter GUS reporter constructs. Both *ATC* and *DHODH* are expressed throughout development in roots, shoots and flowers, in line with previous reports on *ATC*-promoter-GUS studies in Arabidopsis (Chen and Slocum, 2008) or by Northern blots with probes for *de novo* pyrimidine synthesis genes in tobacco (*Nicotiana*

tabacum) leaves (Giermann et al., 2002). Notably, we observed reduced expression of *ATC* and *DHODH* in leaf mesophyll cells of older leaves, suggesting a switch to pyrimidine salvage during aging, largely achieved via uridine/cytidine kinases (Ohler et al., 2019), while expression remained high in leaf veins.

The Target of Rapamycin (TOR) complex is a central growth regulator in plants and animals. Growth requires the constant biosynthesis of ribosomes, which will place a significant demand for nucleotides (Busche et al., 2020). Among the pyrimidine biosynthesis genes, *ATC*, *DHODH* and *CTPS* (encoding CTP synthase) were shown to be upregulated by the glucose-TOR complex (Xiong et al., 2013). Conversely, nucleotide limitation negatively affected TOR activity. It is thus possible that ATC and DHODH may play different roles in the balance between nucleotide pools and TOR activity.

DHODH RNAi lines exhibited reduced growth and seed production, as well as decreased CO_2 assimilation and respiration. By contrast, these lines had close to normal chloroplast ultrastructure, maximal photosynthetic yield and nucleotide levels. However, *DHODH* RNAi lines showed specific responses as well, such as a clear delay in germination. Respiration is the sole energy source during germination. It is therefore tempting to speculate that DHODH may play a regulatory role during respiration. However, current experimental evidence supports an opposite hierarchy, as hypoxic cells with reduced respiration are characterized by pyrimidine deficiency (Wang et al., 2019; Bajzikova et al., 2019). In Arabidopsis, seed hydration is immediately followed by oxygen consumption but also a gradual accumulation of succinate and lactate, possibly reflecting partial hypoxia in embryo tissues after the onset of germination (Nietzel et al., 2019). It is thus possible that germination may be partially characterized by low pyrimidine availability; we would expect *DHODH* RNAi lines to exacerbate this physiological state.

Interestingly, a connection between pyrimidine metabolism and mitochondrial function and morphology was established in human and mouse cell lines, where DHODH inhibitors induced an accumulation of mitochondrial fusion proteins and caused mitochondrial elongation (Löffler et al., 2020). In line with this observation, we detected morphological alterations in mitochondria from *DHODH* knock-down RNAi lines.

Whether DHODH is involved in mitochondrial processes other than oxidizing dihydroorotate during *de novo* pyrimidine synthesis was tested in a study with *Toxoplasma gondii*. This unicellular organism has a DHODH that belongs to the same subfamily as plant DHODHs and is also coupled to the mitochondrial respiratory chain through ubiquinone-mediated oxidation of dihydroorotate (Triana et al., 2016). Whereas supplementation of the

458 growth medium with the salvage substrate uracil did not allow a DHODH loss of function
459 mutant to survive, complementation with a fully catalytically inactive DHODH mutant version
460 was possible. This result indicated that *T. gondii* DHODH is required for a second essential
461 function (Triana et al., 2016). Complementation approaches similar to those tried in *T. gondii*
462 are still out of reach in plants.

463 ## Conclusion

464 In this study, impaired *de novo* pyrimidine synthesis was linked to a low energy state of the
465 knock-down lines, leading to defects in development and growth. Chloroplast-localized ATC
466 exerts a strong control over the pathway, such as ATC protein levels that fall below a threshold
467 markedly affected plastid gene expression and ROS generation. Decreased levels of ATC and
468 DHODH also influenced organellar ultrastructure. The results presented here open new venues
469 for further research on the functional interaction between these two proteins and additional
470 pathways other than *de novo* pyrimidine synthesis (e.g. photosynthesis and respiration).
471
472

Material and Methods

Plant growth

For DNA isolation, tissue collection and phenotypic inspection, wild-type and transgenic *Arabidopsis thaliana* (L.) Heynh. plants (ecotype Columbia) were used throughout. Plants were grown in standardized ED73 (Einheitserde und Humuswerke Patzer) soil or on agar plates under long day conditions in a 14 h light and 10 h dark regime (120 µmol quanta m^{-2} s^{-1}, temperature 22°C, humidity 60%) Illumination was done with LED light (Valoya NS1, Valoya, Finnland). For growth experiments on sterile agar plates, surface-sterilized seeds were grown on half strength MS, supplemented with 0.1% (w/v) sucrose. Prior to germination, seeds were incubated for 24 h in the dark at 4°C for imbibition (Weigel and Glazebrook, 2002). If not stated otherwise, plant material was harvested in the middle of the light period and frozen in liquid nitrogen for further use.

Construction of DHODH knock down plants

For generation of DHODH (*pyrD;* At5g23300) RNAi lines, the procedure described in Wesley et al. (2001) was used. To incorporate the *pyrD* gene fragment in antisense orientation DHODH antisense_fwd and rev primers (Supplemental Table S1) were used. The XbaI/ BamH1 digested PCR fragment was integrated into the corresponding sites of the pHannibal vector. For amplification of the *pyrD* sense fragment DHODH_sense_fwd and rev primers (Supplemental Table S1) were used, and subsequently the PCR product was introduced into pHannibal via XhoI/ EcoRI sites. The gene expression cartridge including a CMV-35S promotor was then introduced into the NotI site of the binary vector pART27 (Gleave, 1992).
All constructs used for Arabidopsis transformation by floral dip (Narusaka et al., 2010) were previously transformed into *A. tumefaciens* strain GV3101 (pMP90; (Furini et al., 1994)).. Several independent, transformed lines were obtained exhibiting different DHODH transcript levels. Two of these (*dhodh#*1 and *dhodh#2*) were selected for further analysis.

RNA extraction and gene expression analysis

Leaf material of soil grown plants was collected and homogenized in liquid nitrogen prior to extraction of RNA with the Nucleospin RNA Plant Kit (Macherey-Nagel, Düren, Germany) according to the manufacturer's advice. RNA purity and concentration were quantified using a Nanodrop spectrophotometer. Total RNA was transcribed into cDNA using the qScript cDNA

Synthesis Kit (Quantabio, USA). qPCR was performed using the quantabio SYBR green quantification kit (Quantabio) on PFX96 system (BioRad, Hercules, CA, USA) using specific primers Supplementary method S1, and At2g3760 (Actin) was used as reference gene for transcript normalization. At least three biological replicates were analyzed. Mean values and standard errors were calculated from at least three biological replicates.

Protein extraction and immunoblotting

Leaf extract of wild type and mutants was prepared by homogenizing leaf material in extraction buffer (50 mM HEPES-KOH, pH 7.2, 5 mM MgCl2, 2 mM phenylmethylsulfonyl fluoride (PMSF)) on ice. This homogenous extract was centrifuged for 10 min, 20,000g and 4°C. The supernatant was collected and stored on ice until use.

For immunoblotting 15 µg of a protein extract from Arabidopsis leaves separated in a 15% SDS-PAGE gel were transferred onto a nitrocellulose membrane (Whatman, Germany) by wet blotting. The membrane was blocked in phosphate-buffered saline plus 0.1% [v/v] Tween 20 (PBS-T) with 3% milk powder for 1 h at room temperature, followed by three washes of 10 min in PBS-T. Then, the membrane was incubated with a rabbit polyclonal antiserum raised against recombinant ATC (Eurogentec, Belgium) for 1 h, followed by three washes with PBS-T. Antibodies against photosynthetic proteins (PsaA #AS06172100, PsbA #AS05084, PsbD #AS06146, lhcb2 #AS01003, lhca1 #AS01005, AtpB #AS05085, cytb6-PetB #AS148169) were purchased from Agrisera (Vännäs, Sweden) Next, the membrane was incubated for 1 h with a horseradish peroxidase (HPR) conjugated anti-rabbit antibody (Promega, Walldorf, Germany) diluted in PBS-T with 3% milk powder. The result was visualized by chemiluminescence using the ECL Prime Western blotting reagent (GE Healthcare) and a Fusion Solo S6 (Vilber-Lourmat) imager.

Chlorophyll analysis

Photosynthetic pigments were extracted from ground leave tissue with 90% acetone/ 10% 0.2 M Tris/HCl pH 7.5 for 48h at 4°C in the dark. Chlorophyll were measured by the absorbance of the supernatant at 652 nm. The quantification was performed as described by Arnon (1949).

Generation of constructs and staining for GUS Activity

For the histochemical localization of promoter activity of *PYRB* and *PYRD*, a 965 bp upstream fragment of *PYRB* (ATC) was inserted to pBGWFS7 (Karimi et al., 2002) using the primers ATC_gus_fwd and ATC_gus_rev and a 1140 bp upstream fragment of *PYRD* (DHODH) was

inserted to pGPTV (Becker et al., 1992) using the primers DHODH_gus_fwd and DHODH_gus_rev (Supplemental Table 1). The resulting constructs were transformed in *Agrobacterium* strain GV3101. Transformation of *Arabidopsis* was conducted according to the floral dip method (Clough and Bent, 1998). Tissue from transgenic plants was collected in glass vials, filled with ice-cold 90% acetone, and incubated for 20 min at room temperature. Subsequently, the samples were stained according to standard protocols (Weigel and Glazebrook, 2002).

Germination assays and root growth tests

Seed germination was analyzed with three petri dishes per genotype (each with 40 seeds) and 3 replications of the complete experiment. Seeds were grown on agar plates starting at the onset of light. After indicated time points seeds were inspected for radicle protrusion. For root growth seeds were treated as indicated above and grown vertically on square (120 × 120 mm) petri plates. 20 seeds per genotype were inspected in parallel and the experiment was repeated 3 times. Root length of seven days old seedlings was measured after scanning of agar plates with help of ImageJ software.

Light- and electron microscopy

For image analysis of freshly prepared siliques, a Keyence VHX-5000 digital microscope (Keyence Germany GmbH, Neu-Isenburg, Germany) has been used. For histological and ultrastructural examinations, combined conventional and microwave-assisted fixation, substitution, and resin embedding of 2mm^2 leaf cuttings were performed using a PELCO e BioWave® Pro+ (TedPella, Redding, CA, USA), according to Supplementary method S2. Therefore 4-6 cuttings of the central part of 2 different rosette leaves of at least 4 different WT and mutant plants were used. Sectioning of resin blocks, histological staining, light- and electron microscopical analysis has been carried out as described previously (Daghma et al., 2011).

PAM measurements

A MINI-IMAGING-PAM fluorometer (Walz Instruments, Effeltrich, Germany) was used for *in vivo* chlorophyll A light curve assays on intact, 6-week-old dark-adapted plants using standard settings (Schreiber et al., 2007). Measurements were performed with eight plants per line in light curves recorded by incrementally increasing light pulses with intensity from PAR (µmol photons m^{-2} s^{-1}) 0 to PAR 726 in 14 steps.

565

566 **Gas exchange measurements**

567 Plants were grown for 6 weeks on soil in a 10h/ 14h light and dark regime. Gas exchange-
568 related parameters were analyzed with a GFS-3000 system (Heinz Walz, Effeltrich, Germany).
569 Measurements were performed with six plants per condition and each plant was measured three
570 times (technical replicates). Individual plants were placed in a whole plant gas exchange
571 cuvette and CO_2-assimilation rate, respiration, leaf CO_2 concentration, and stomatal
572 conductance were recorded. Temperature, humidity, and CO_2 concentrations of the cuvette
573 were set to the condition's plants were grown at. Light respiration was measured at PAR 125
574 and dark respiration at PAR 0 over a time of 1 min for each plant. Each plant was measured
575 three times with 30 seconds intervals between measurement to allow leaves to return to the
576 stabilized value.

577 **Superoxide and H_2O_2 staining**

578 Superoxide and H2O2 staining were visually detected with nitro blue tetrazolium (NBT) and
579 3,3'-diaminobenzidine (DAB). In situ detection of O^{2-} was performed by treating plants with
580 NBT as previously described by Wohlgemuth et al. (2002).
581 *A. thaliana* leaves were vacuum-infiltrated with 0.1% NBT 50 mM potassium phosphate buffer
582 (pH 7.8) and 10 mM sodium-azide for 20 minutes and incubated for 1 h at room temperature.
583 Stained leaves were boiled in 95% Ethanol for 15 minutes and photographed. Detection of
584 H_2O_2 was performed by treating plants with DAB-HCl as previously described by Fryer et al.
585 (2002).
586 Leaves were vacuum-infiltrated with 5 mM DAB-HCl, pH 3, for 20 min, and incubated in the
587 same solution for at least 8 hours overnight. Stained leaves were boiled in an ethanol:acetic
588 acid:glycerol (3:1:1) solution under the hood until they turned transparent and were later
589 photographed.

590 **Whole-leaf ascorbate determination**

591 Whole-leaf samples from three independent plants (6 weeks old) per genotype were harvested,
592 weighed, and immediately ground in liquid nitrogen after 6 hours under the prevailing 14h
593 light/ 10h dark regime. Ascorbate and dehydroascorbate levels were determined
594 colorimetrically as described previously by Gillespie and Ainsworth (2007).
595

Metabolite Extraction and Quantification LC-MS

For the metabolite profiling, the freeze-dried and homogenized samples were extracted according to Schwender et al., (2015). Untargeted profiling of anionic central metabolites was performed using the Dionex-ICS-5000+HPIC the ion chromatography system (Thermo Scientific) coupled to a Q-Exactive Plus hybrid quadrupol-orbitrap mass spectrometer (Thermo Scientific). The detailed chromatographic and MS conditions are described in the Supplementary Method S3. The randomized samples were analyzed in full MS mode. The data-dependent MS-MS analysis for the compound identification was performed in the pooled probe, which also was used as a quality control (QC). The batch data was processed using the untargeted metabolomics workflow of the Compound Discoverer 3.0 software (Thermo Scientific). The compounds were identified using the inhouse library, as well as a public spectral database mzCloud and the public databases KEGG, NIST and ChEBI via the mass- or formula-based search algorithm. The P-values of the group ratio were calculated by ANOVA and a Tukey-HCD post hoc analysis.

Adjusted P-values were calculated using Benjamini-Hochberg correction. Untargeted profiling of amino acids and other cationic metabolites was performed using the Vanquish Focused ultra-high-pressure liquid chromatography (UHPLC) system (Thermo Scientific) coupled to a QExactive Plus mass spectrometer (Thermo Scientific). The detailed chromatographic and MS conditions are described in the Supplementary Method S2. The batch processing and compound identification workflow was essentially the same as described for the IC-MS-based untargeted profiling.

ACCESSION NUMBERS

ATC (*pyrB;* At3g20330); DHODH (*pyrD;* At5g23300)

SUPPLEMENTAL DATA

635 **ACKNOWLEDGEMENTS**

636 We thank Marion Benecke, Claudia Riemey and Kirsten Hoffie (IPK Gatersleben) for technical
637 assistance with sample preparation for histology and electron microscopy. We thank Hardy
638 Rolletscheck for advice and support in metabolite analysis. Furthermore, we are indebted to
639 Monika Löffler and Wolfgang Knecht for fruitful discussions and critical reading of the
640 manuscript. This work was funded by DFG grants (CRC Transregio TRR175, A03 to J.M. and
641 B08 and IRTG1830 to T.M).

642

643 # LITERATURE CITED

644 **Arnon DI** (1949): Copper enzymes in isolated chloroplasts. Polyphenoloxidase in Beta
645 vulgaris. *Plant Physiol* **24**: 1-15.

646 **Bajzikova, M., Kovarova, J., Coelho, A. R., Boukalova, S., Oh, S., Rohlenova, K., Svec,**
647 **D., Hubackova, S., Endaya, B., Judasova, K. et al. (2019**). Reactivation of
648 dihydroorotate dehydrogenase-driven pyrimidine biosynthesis restores tumor growth of
649 respiration-deficient cancer cells. *Cell metabolism* 29: 399-416.

650 **Becker D, Kemper E, Schell J, Masterson R** (1992). New plant binary vectors with selectable
651 markers located proximal to the left T-DNA border. Plant Mol Biol **20:** 1195-1197.

652 **Bellin L, del Caño-Ochoa F, Velázquez-Campoy A, Möhlmann T, Ramón-Maiques S**
653 (2021). UMP inhibition and sequential firing in aspartate transcarbamoylase open ways
654 to regulate plant growth. *Nature Communications, in press*

655 **Brunkard J O** (2020). Exaptive Evolution of Target of Rapamycin Signaling in Multicellular
656 Eukaryotes. *Developmental Cell*. doi: https://doi.org/10.1016/j.devcel.2020.06.022

657 **Brychkova G, Alikulov Z, Fluhr R, Sagi M** (2008) A critical role for ureides in dark and
658 senescence-induced purine remobilization is unmasked in the Atxdh1 Arabidopsis
659 mutant. *Plant J* **54**: 496–509

660 **Busche M, Scarpin MR, Hnasko R, Brunkard JO** (2020). TOR coordinates nucleotide
661 availability with ribosome biogenesis in plants. *bioRxiv. doi: https://doi.org/*
662 *10.1101/2020.01.30.927418*

663 **Carrillo LR, Froehlich JE, Cruz JA, Savage LJ, Kramer DM** (2016). Multi-level regulation
664 of the chloroplast ATP synthase: the chloroplast NADPH thioredoxin reductase C
665 (NTRC) is required for redox modulation specifically under low irradiance. *Plant J* **87**:
666 654-663.

667 **Christopherson RI, Szabados E** (1997). Nucleotide biosynthesis in mammals. *PORTLAND*
668 *PRESS RESEARCH MONOGRAPH*, 315-335.

669 **Clough SJ, Bent AF** (1998). Floral dip: a simplified method for Agrobacterium-mediated
670 transformation of Arabidopsis thaliana. *Plant J* **16**: 735-743.

671 **Daghma DS, J Kumlehn Melzer M** (2011)The use of cyanobacteria as filler in nitrocellulose
672 capillaries improves ultrastructural preservation of immature barley pollen upon high
673 pressure freezing. *J Microsc* **244**: 79-84

674 **Doremus HD, Jagendorf AT** (1985). Subcellular localization of the pathway of de novo
675 pyrimidine nucleotide biosynthesis in pea leaves. *Plant Physiol* **79**: 856-861.

676 **Foyer CH, Noctor G** (2011). Ascorbate and glutathione: the heart of the redox hub. *Plant*
677 *Physiol* **155**: 2-18.

678 **Fryer MJ, Oxborough K, Mullineaux PM, Baker NR** (2002). Imaging of photo-oxidative
679 stress responses in leaves. *J Exp Bot* **53**: 1249-1254.

680 **Furini A, Koncz C, Salamini F, Bartels D** (1994). Agrobacterium-mediated transformation
681 of the desiccation-tolerant plant Craterostigma plantagineum. *Plant Cell Rep* **14**: 102-
682 106.

683 **Garavito MF, Narváez-Ortiz HY, Zimmermann BH** (2015). Pyrimidine metabolism:
684 dynamic and versatile pathways in pathogens and cellular development. *JGG* **42**: 195-
685 205.

686 **Geigenberger P, Regierer B, Nunes-Nesi A, Leisse A, Urbanczyk-Wochniak E, Springer**
687 **F, van Dongen JT, Kossmann J Fernie AR** (2005) Inhibition of de novo pyrimidine

synthesis in growing potato tubers leads to a compensatory stimulation of the pyrimidine salvage pathway and a subsequent increase in biosynthetic performance. *Plant Cell*, **17**: 2077-2088.

Giermann N, Schröder M, Ritter T, Zrenner R (2002). Molecular analysis of de novo pyrimidine synthesis in solanaceous species. Plant Mol. Biol. **50**: 393-403.

Gillespie KM, Ainsworth EA (2007). Measurement of reduced, oxidized and total ascorbate content in plants. *Nature Protocols*, **2**: 871-874.

Gleave AP (1992). A versatile binary vector system with a T-DNA organisational structure conducive to efficient integration of cloned DNA into the plant genome. *Plant Mol Biol* **20**: 1203-1207.

Järvi S, Suorsa M, Aro EM (2015). Photosystem II repair in plant chloroplasts—regulation, assisting proteins and shared components with photosystem II biogenesis. *Biochim Biophys Acta (BBA)-Bioenergetics* **1847**: 900-909.

Kafer C, Zhou L, Santoso D, Guirgis A, Weers B, Park S, Thornburg R (2004) Regulation of pyrimidine metabolism in plants. *Front Biosci* **9**: 1611–1625

Karimi M, Inzé D, Depicker A (2002). GATEWAY™ vectors for Agrobacterium-mediated plant transformation. *TIPS* **7**: 193-195.

Kato Y, Miura E, Ido K, Ifuku K, Sakamoto W (2009). The variegated mutants lacking chloroplastic FtsHs are defective in D1 degradation and accumulate reactive oxygen species. *Plant Physiol* **151**: 1790-1801.

Kim H, Kelly RE, Evans DR. (1992) The structural organization of the hamster multifunctional protein CAD. Controlled proteolysis, domains, and linkers. J. Biol. Chem. **267**: 7177-7184.

Lambrev PH, Miloslavina Y, Jahns P, Holzwarth AR (2012). On the relationship between non-photochemical quenching and photoprotection of Photosystem II. Biochim Biophys Acta, **1817**: 760-769.

Lehninger AL, Nelson DL, Cox MM (1994). Prinzipien der Biochemie, H. Tschesche, ed (Heidelberg, Berlin, Oxford: *Spektrum Akademischer Verlag*).

Löffler M, Carrey EA, Knecht W (2020). The pathway to pyrimidines: The essential focus on dihydroorotate dehydrogenase, the mitochondrial enzyme coupled to the respiratory chain. *Nucleosides, Nucleotides and Nucleic Acids*, 1-25.

Martinussen J, Willemoës M, Kilstrup M (2011). Nucleotide Metabolism. In: M. Moo-Young (Ed.), Comprehensive Biotechnology (2 ed., Vol. 1, pp. 91-107). Elsevier.http://www.sciencedirect.com/science/referenceworks/9780080885049#ancsec1

Moffatt BA, Ashihara H (2002). Purine and pyrimidine nucleotide synthesis and metabolism. The Arabidopsis Book/American Society of Plant Biologists, 1.

Nara T, Hshimoto T, Aoki T (2000). Evolutionary implications of the mosaic pyrimidine-biosynthetic pathway in eukaryotes. *Gene* **257**: 209-222.

Narusaka M, Shiraishi T, Iwabuchi M, Marusaka Y (2010). The floral inoculating protocol: A simplified Arabidopsis thaliana transformation method modified from floral dipping. *Plant Biotech* **27**: 349-351.

Nasr F, Bertauche N, Dufour ME, Minet M, Lacroute F (1994). Heterospecific cloning of Arabidopsis thaliana cDNAs by direct complementation of pyrimidine auxotrophic mutants of Saccharomyces cerevisiae. I. Cloning and sequence analysis of two cDNAs

catalysing the second, fifth and sixth steps of the de novo pyrimidine biosynthesis pathway. *MGG* **244**: 23-32.

Nietzel T, Mostertz J, Ruberti C, Née G, Fuchs P, Wagner S, Moseler A, Müller-Schüssele SJ, Benamar A, Poschet G et al. (2020) Redox-mediated kick-start of mitochondrial energy metabolism drives resource-efficient seed germination. Proc Natl Acad Sci **117**: 741-751.

Noctor G, Foyer CH (1998). Ascorbate and glutathione: keeping active oxygen under control. *Annu Rev Plant Biol* **49**: 249-279.

Ohler L, Niopek-Witz S, Mainguet SE, Möhlmann, T (2019). Pyrimidine salvage: Physiological functions and interaction with chloroplast biogenesis. *Plant Physiol* **180**: 1816-1828.

Queval G, Noctor G (2007). A plate reader method for the measurement of NAD, NADP, glutathione, and ascorbate in tissue extracts: application to redox profiling during Arabidopsis rosette development. Anal Biochem 363: 58-69.

Rottet S, Besagni C, Kessler F. (2015) The role of plastoglobules in thylakoid lipid remodeling during plant development. *Biochim Biophys Acta* **1847**: 889–899

Santoso D, and Thornburg, R. (1998). Uridine 5′-monophosphate synthase is transcriptionally regulated by pyrimidine levels in Nicotiana plumbaginifolia. *Plant Physiol* **116**: 815-821.

Schmid, LM, Ohler L, Möhlmann T, Brachmann A, Muiño JM, Leister D, Meurer J Manavski N (2019). PUMPKIN, the sole plastid UMP kinase, associates with group II introns and alters their metabolism. *Plant Physiol* **179**: 248-264.

Schreiber U, Quayle P, Schmidt S, Escher BI, Mueller JF (2007) Methodology and evaluation of a highly sensitive algae toxicity test based on multiwell chlorophyll fluorescence imaging. *Biosens Bioelectron* **22**: 2554–2563

Schröder M, Giermann N, Zrenner R (2005) Functional analysis of the pyrimidine de novo synthesis pathway in solanaceous species. *Plant Physiol* **138**: 1926–1938

Schwender J, Hebbelmann I, Heinzel N, Hildebrandt T, Rogers A, Naik D, Klapperstück M, Braun HP, Schreiber F, Denolf P et al. (2015). Quantitative multilevel analysis of central metabolism in developing oilseeds of oilseed rape during in vitro culture. Plant Physiol **168**: 828-848.

Stitt M, Lilley RMcC, Gerhardt R, Heldt HW (1989). Metabolite levels in specific cells and subcellular compartments of plant leaves. In: *Methods in Enzymology* (Academic Press) **32**: 518–552.

Su J, Yang L, Zhu Q, Wu H, He Y, Liu Y, et al. (2018) Active photosynthetic inhibition mediated by MPK3/MPK6 is critical to effector-triggered immunity. PLoS Biol 16: e2004122. https://doi.org/10.1371/journal.pbio.2004122

Triana MAH, Herrera DC, Zimmermann BH, Fox BA, Bzik DJ (2016). Pyrimidine pathway-dependent and-independent functions of the *Toxoplasma gondii* mitochondrial dihydroorotate dehydrogenase. *Infection and immunity*, **84**: 2974-2981.

Trentmann O, Mühlhaus T, Zimmer D, Sommer F, Schroda M, Haferkamp I, Keller I, Pommerrenig B, Neuhaus HE (2020). Identification of chloroplast envelope proteins with critical importance for cold acclimation. *Plant Physiol* **182**: 1239-1255.

Ullrich A, Knecht W, Piskur J, Löffler M (2002). Plant dihydroorotate dehydrogenase differs significantly in substrate specificity and inhibition from the animal enzymes. *FEBS Lett* **529**: 346-350.

Wang Y, Bai C, Ruan Y, Liu M, Chu Q, Qiu L, Yang C, Li B (2019) Coordinative metabolism of glutamine carbon and nitrogen in proliferating cancer cells under hypoxia. Nat Commun **14**: 201. doi: 10.1038/s41467-018-08033-9.

Weigel D, Glazebrook J (2002). Arabidopsis. A laboratory manual (New York, NY: *Cold Spring Harbor Laboratory Press*).

Wesley SV, Helliwell CA, Smith NA, Wang MB, Rouse DT, Liu Q, Gooding PS, Singh, SP, Abbott D, Stoutjesdijk PA, et al. (2001). Construct design for efficient, effective and high-throughput gene silencing in plants. *Plant J* **27**: 581-590.

Williamson CL, Slocum RD (1994). Molecular cloning and characterization of the pyrB1 and pyrB2 genes encoding aspartate transcarbamoylase in pea (*Pisum sativum L.*). *Plant Physiol*, **105**: 377-384.

Williamson CL, Lake MR, Slocum RD (1996). A cDNA encoding carbamoyl phosphate synthetase large subunit (carB) from Arabidopsis (Accession No. U40341)(PGR96-055). *Plant Physiol* **111,** 1.

Witz S, Jung B, Fürst S, Möhlmann T (2012). De novo pyrimidine nucleotide synthesis mainly occurs outside of plastids, but a previously undiscovered nucleobase importer provides substrates for the essential salvage pathway in Arabidopsis. *Plant Cell* **24**: 1549-1559.

Witte CP, Herde M (2020). Nucleotide metabolism in plants. *Plant Physiol*, **182**: 63.

Wohlgemuth H, Mittelstrass K, Kschieschan S, Bender J, Weigel HJ, Overmyer K, Kangasjarvi J, Sandermann H, Langebartels, C (2002). Activation of an oxidative burst is a general feature of sensitive plants exposed to the air pollutant ozone. *Plant, Cell and Environment*, **25**: 717-726.

Xiong Y, McCormack M, Li L, Hall Q, Xiang C, Sheen J (2013). Glucose–TOR signalling reprograms the transcriptome and activates meristems. *Nature* **496**: 181-186.

Zrenner R, Stitt M, Sonnewald U, Boldt R. (2006). Pyrimidine and purine biosynthesis and degradation in plants. *Annu Rev Plant Biol* **57** : 805-836.